



Cite this: *RSC Adv.*, 2017, 7, 44659

Effects of La, Sm and Yb doping on thermoelectric properties of $\text{Ca}_{0.98}\text{Er}_{0.02}\text{MnO}_3$ at high temperature

Tao Yang  and Tiexin Cheng *

A series of perovskite-type ceramic materials $\text{Ca}_{0.98}\text{Er}_{0.02}\text{MnO}_3$ (CDM) and $\text{Ca}_{0.96}\text{Er}_{0.02}\text{Re}_{0.02}\text{MnO}_3$ (Re = La, Sm, Yb) (denoted as CDM-La, CDM-Sm, CDM-Yb) which worked from 300 K to 1000 K with excellent thermoelectric properties was prepared by a sol-gel and cold-pressing method. XRD results revealed that the prepared samples are uniform crystalline particles with high purity. The results of XPS characterization show that an increase in the Mn^{3+} ratio is caused by the introduction of dual-doping. The characterization results of resistivity and Seebeck coefficient reveal that the carrier concentration is optimized by dual doping, accordingly the resistivity decreases continuously and the value of the Seebeck coefficient increases continuously. The highest power factor of $219 \mu\text{W} (\text{K}^2 \text{m})^{-1}$ is obtained at 773 K for the $\text{Ca}_{0.96}\text{Er}_{0.02}\text{Yb}_{0.02}\text{MnO}_3$ sample. And also the introduction of a second element contributes to lower the thermal conductivity. The highest figure of merit, ZT , of the $\text{Ca}_{0.96}\text{Er}_{0.02}\text{Yb}_{0.02}\text{MnO}_3$ sample exceeds 0.12 at 973 K.

Received 31st July 2017
Accepted 10th September 2017

DOI: 10.1039/c7ra08446c

rsc.li/rsc-advances

1. Introduction

Thermoelectric materials can direct transfer energy between heat and electricity. They are a promising means for reliable and simple energy saving. Thermoelectric performance is determined in general by calculating a material's dimensionless figure of merit ZT , defined as $ZT = S^2\sigma T/\kappa$, where S is the Seebeck coefficient, σ is the electrical conductivity, κ is the total thermal conductivity, T is the absolute temperature in Kelvin, and the product $S^2\sigma$ is the power factor.

Thermoelectric oxides are a representative class of thermoelectric materials. For a long time, many thermoelectric oxides with high thermoelectric performance have been researched, such as NaCo_2O_4 , $\text{Ca}_3\text{Co}_4\text{O}_{9-\delta}$, $\text{Bi}_2\text{Sr}_2\text{Co}_2\text{O}_y$, $\text{TiSr}_2\text{Co}_2\text{O}_y$, SrTiO_3 .^{1–5} But there are few n-type oxide thermoelectric materials to be reported, where the ZT of n-type is significantly higher than that of p-type.²⁵ CaMnO_3 has attracted attention as a prospective candidate of n-type thermoelectric oxides.^{6–8} Thermoelectric correlation parameters of CaMnO_3 were first researched by Takizawa *et al.*⁹ and Ohtaki *et al.*¹⁰ It is reported that the largest power factor of $\text{Ca}_{0.9}\text{Bi}_{0.1}\text{MnO}_3$ attains $2.8 \times 10^{-4} \text{ W m}^{-1} \text{ K}^{-2}$ at 1073 K and samples show a maximum ZT value of 0.085 at 1173 K. On the basis of their study, doping with some other trivalent elements were reported by Funahashi *et al.*^{11,12} It is reported that the highest power factor achieved $0.22 \text{ mW m}^{-1} \text{ K}^{-2}$ at 773 K and the highest dimensionless figure of merit obtained was 0.09 at 973 K. It can be seen that doping is an effective way to reduce resistivity. According to these studies,

the Wang *et al.*^{13–15} reported lanthanide elements substitution with a higher doping level of 10%, then they studied a large thermoelectric performance of CaMnO_3 by doping Dy at Ca site and achieved $ZT = 0.2$ in $\text{Ca}_{0.9}\text{Yb}_{0.1}\text{MnO}_3$. Bhaskar *et al.*¹⁶ and Liu *et al.*¹⁷ found that a lower Dy doping could be exhibited an antiferromagnetic transition in CaMnO_3 . But most studies have been focused on the single doping for CaMnO_3 system. And following experiments, Zhu *et al.*¹⁸ reported the thermoelectric performance of Er and Dy dual doped CaMnO_3 and achieved $ZT = 0.23$ in $\text{Ca}_{0.96}\text{Er}_{0.02}\text{Dy}_{0.02}\text{MnO}_3$. As we all know, Er and Dy have similar atomic structures and similar ionic radii. Herein, a series of perovskite-type ceramic materials $\text{Ca}_{0.98}\text{Er}_{0.02}\text{MnO}_3$ (CDM) and $\text{Ca}_{0.96}\text{Er}_{0.02}\text{Re}_{0.02}\text{MnO}_3$ (Re = La, Sm, Yb) (denoted CDM-La, CDM-Sm, CDM-Yb) which prepared by sol-gel method, and $\text{Ca}_{0.98}\text{Er}_{0.02}\text{MnO}_3$ (CDM) as a comparison. Those samples were evaluated from 300 K to 1000 K.

2. Experimental procedure

Sol-gel and cold pressing method was used to synthesize samples of $\text{Ca}_{0.98}\text{Er}_{0.02}\text{MnO}_3$ and $\text{Ca}_{0.96}\text{Er}_{0.02}\text{Re}_{0.02}\text{MnO}_3$ ceramics, with Re = La, Sm, Yb. The starting materials were $\text{Ca}(\text{NO}_3)_2$ (99.0%), $\text{Mn}(\text{NO}_3)_2$ solution (50.0%), Er_2O_3 (99.9%), La_2O_3 (99.9%), $\text{Sm}(\text{NO}_3)_3$ (99.8%), $\text{Yb}(\text{NO}_3)_3$ (99.8%), $\text{C}_2\text{H}_6\text{O}_2$ (95.0%) and $\text{C}_6\text{H}_8\text{O}_7$ (99.0%). All raw materials were provided by Sinopharm Group Co., Ltd., weighed in stoichiometric proportions and added into deionized water. Evaporation for 7 h at 325 K under gentle stirring afforded a purple solution, which was transformed into a yellow gel precursor after drying at 473 K for 2 h. After the wet mixtures dried, the powder was calcinated for 12 h at 1423 K in ambient atmospheric condition with an

College of Chemistry, Jilin University, Changchun, Jilin, 130021, China. E-mail: hign1@outlook.com

intermediate grinding. The calcined powder was ball-milled for 12 h to obtain a fine powder. The ground powder was tableted at 30 MPa under air atmosphere, and sintered in air at 1573 K for 12 h. The ceramics were cut into rectangular columns with dimensions of 3 mm × 4 mm × 8 mm for measurement of thermoelectric properties.

X-ray powder diffraction (XRD) analysis was carried out using a Rigaku D/max-rA X-ray diffractometer with Cu K α radiation and scanning (a step width of 2°) over the angular range 20 to 70°. The electrical resistivity (ρ) and Seebeck coefficients (S) were measured simultaneously using a ZEM-1 apparatus in the temperature range between 300 and 1000 K. The carrier concentration was measured by HL5500 at room temperature. Thermal conductivity values (κ) were calculated from the thermal diffusivity (λ), the specific heat capacity (C_p), and the density (d) by applying the following relationship: $\kappa = \lambda C_p d$. The density of the samples was measured by the Archimedes method. The thermal diffusivity and specific heat capacity were measured with a laser flash apparatus (Netzsch LFA 457) and different thermal analyzers (Netzsch Q20-DSC), respectively. The power factor, figure of merit ZT , Hall coefficient, mobility and theoretical density were calculated.

3. Results and discussion

The XRD patterns of CDM, CDM-La, CDM-Sm and CDM-Yb were presented at room temperature in Fig. 1. The diffraction peaks of the prepared doping samples are identical with those in the standard JCPDS (89-0666) card of CaMnO_3 (ref. 19) and all samples have without any second phase occurs. Based on results showed that the Er^{3+} , La^{3+} , Sm^{3+} and Yb^{3+} ions have entered into the CaMnO_3 lattice. According to the XRD data, lattice parameters and theoretical density shown listed in Table 1. From which can be seen directly that lattice parameters of CDM is smaller than dual doped samples. However, we have known that the ionic radius of Ca^{2+} (1.12 Å) is larger than that of Sm^{3+} (1.079 Å) and Yb^{3+} (1.008 Å)²⁴ ions and only Ca^{2+} is a little smaller than that of La^{3+} (1.16 Å) ions.²⁰ Fig. 2 shows XPS Mn 2p

spectra of CaMnO_3 and CDM-Sm. The Mn 2p_{3/2} characteristic peaks of the CaMnO_3 sample split into two peaks of 642.3 eV and 641.5 eV, which are close to the binding energy of Mn^{4+} and Mn^{3+} , which indicates that the Mn ions exist in the two chemical valence states in the CaMnO_3 . The Mn 2p characteristic peaks of the CDM-Sm samples showed only a broad peak at 641.6 eV, which is close to the binding energy of Mn^{3+} , this shows that the dual-doping makes the composition of Mn^{3+} to increase. The doping causes the charge imbalance, in order to maintain the electrically neutral, Mn ions change the chemical valence to balance the excess charge. It is known that there are two different sizes in the ionic radii between Mn^{3+} (0.645 Å) and Mn^{4+} (0.530 Å) in the system.²⁰ Therefore, the variation of lattice parameters is due to the increase of Mn^{3+} . The similar results have been reported by Wang *et al.*⁵ For the orthorhombic perovskite structure of ABO_3 type, the distortion of the structure leads to the lattice constant becoming orthorhombic structure from the cubic structure. As can be seen from Table 1, all samples of a , b , c values are satisfied $c < b/\sqrt{2} < a$ relationship, which indicates that the sample is O-type orthorhombic structure.

Table 2 gives the EDX analysis results of $\text{Ca}_{0.98}\text{Er}_{0.02}\text{MnO}_3$ and $\text{Ca}_{0.96}\text{Er}_{0.02}\text{Re}_{0.02}\text{MnO}_3$ (Re = La, Sm, Yb). Experimental densities are 4.382 g cm⁻³, 4.396 g cm⁻³, 4.410 g cm⁻³ and 4.412 g cm⁻³ for samples of CDM, CDM-La, CDM-Sm, and CDM-Yb, respectively. From Table 1, it can be seen directly that the ever-increasing atomic number makes the measured density also larger, which is due to the contribution from the heavier mass of La, Sm, and Yb elements. The relative densities, defined as the experimental density over the theoretical density, are all 92.5–93.2%, which means the samples are of good compactness.

The temperature dependence of resistivity for CDM, CDM-La, CDM-Sm, and CDM-Yb is shown in Fig. 3. This samples exhibit metal-like characteristics, the resistivity increases with increasing temperature ($d\rho/dT > 0$) throughout the whole test temperature range. The similar phenomenon is reported by Wang *et al.* and Liu *et al.*^{14–18} The resistivity is 36.5 mΩ cm, 14.1 mΩ cm, 13.1 mΩ cm and 12.3 mΩ cm, for CDM, CDM-La, CDM-Sm and CDM-Yb, respectively at 973 K. It is apparent the resistivity of CDM decreases significantly when the second element are doped. All samples have no visible difference. As we all know, the carrier concentration and mobility limit the resistivity, in Fig. 3 the resistivity of the three dual-doping samples have a similar trend, it can be concluded that the carrier concentration and mobility of the three samples also have the similar trend.

From Table 3, the carrier concentration is obtained from the measured Hall coefficient. It can be expressed as $R_H = 1/ne$, where R_H , n and e are the Hall coefficient, carrier concentration and electron charge, respectively. The doping of the second element increases the carrier concentration for the system. The mobility is calculated from the carrier concentration and the electrical conductivity according to $\sigma = ne\mu$. Since the conductivity and carrier concentration of CDM-Yb are relatively large, the mobility is also the highest.

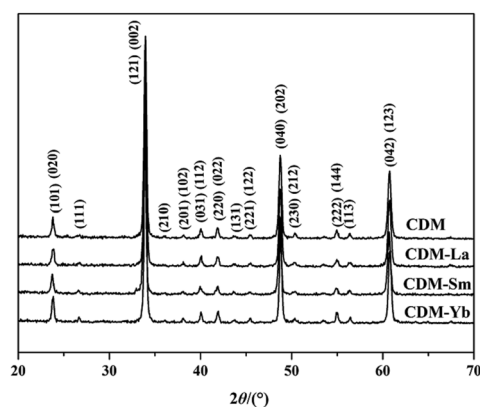
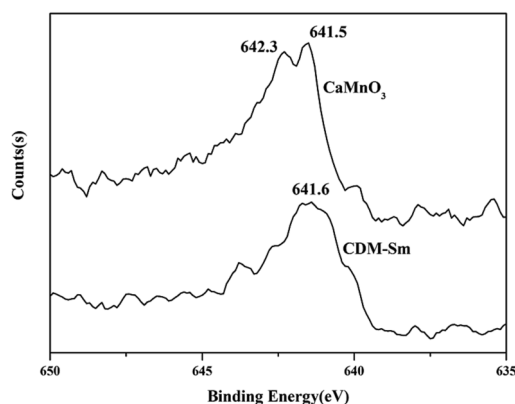


Fig. 1 Room temperature X-ray diffraction patterns for $\text{Ca}_{0.98}\text{Er}_{0.02}\text{MnO}_3$ and $\text{Ca}_{0.96}\text{Er}_{0.02}\text{Re}_{0.02}\text{MnO}_3$ (Re = La, Sm, Yb).



Table 1 Lattice parameters, densities of $\text{Ca}_{0.98}\text{Er}_{0.02}\text{MnO}_3$ and $\text{Ca}_{0.96}\text{Er}_{0.02}\text{Re}_{0.02}\text{MnO}_3$ (Re = La, Sm, Yb)

Samples	<i>a</i> (Å)	<i>b</i> (Å)	<i>c</i> (Å)	Theoretical density (g cm ⁻³)	Experimental density (g cm ⁻³)	Relative density (%)
CDM	5.438	7.487	5.291	4.701	4.382	93.2
CDM-La	5.449	7.501	5.299	4.738	4.396	92.7
CDM-Sm	5.451	7.504	5.303	4.744	4.410	92.9
CDM-Yb	5.453	7.505	5.303	4.765	4.412	92.5

**Fig. 2** XPS Mn 2p spectra of CaMnO_3 and CDM-Sm.

Usually, the resistivity of perovskite type acid salt can be expressed as

$$\rho = \frac{C}{T} \exp\left(-\frac{E_a}{\kappa_B T}\right) \quad (1)$$

where C , T , E_a , and κ_B , are material dependent constant, absolute temperature, activation energy and Boltzmann constant, respectively. The conductive mechanism of the material can be determined by the $\ln(\sigma T)$ and $1000/T$ relation curve. Temperature dependence of $\ln(\sigma T)$ and $1000/T$ relation curve for CDM, CDM-La, CDM-Sm, and CDM-Yb ceramics is shown in Fig. 4. The curves of all samples showed good linear correlation, similar curves was also reported in other doped samples,^{22,23} It is shown that this is a typical small polaron hopping conduction behavior. Through the calculation, the activation energy of the CDM sample is 0.28 eV and the $\text{Ca}_{0.96}\text{Er}_{0.02}\text{Re}_{0.02}\text{MnO}_3$ (Re = La, Sm, Yb) sample is 0.20 eV, 0.23 eV, 0.18 eV, respectively. It can be seen from the calculation results that with the introduction of second kinds of impurity elements, the activation energy of materials decreases, which shows that double interaction can further reduce the activation energy of materials. The sample

Table 2 EDX results showing the elemental weight (%) of $\text{Ca}_{0.98}\text{Er}_{0.02}\text{MnO}_3$ and $\text{Ca}_{0.96}\text{Er}_{0.02}\text{Re}_{0.02}\text{MnO}_3$ (Re = La, Sm, Yb)

Sample	Ca%	Er%	La%	Sm%	Yb%	Mn%	O%	Pt%
CDM	30.82	4.89	0	0	0	38.26	25.82	0.21
CDM-La	31.43	2.95	1.96	0	0	36.56	26.72	0.38
CDM-Sm	28.89	2.71	0	2.21	0	37.71	28.26	0.22
CDM-Yb	30.41	2.89	0	0	2.37	39.91	24.17	0.25

with double percolation has smaller activation energy, indicating that the band gap of the band structure is narrower, indicating that the double percolation is a narrow band semiconductor. This result shows that dual doping leads to a substantial decrease of the activation energy, which induces an increase in electrical conductivity over that of CaMnO_3 .

The Seebeck coefficients of CDM, CDM-La, CDM-Sm, and CDM-Yb ceramics as a function of temperature were displayed in Fig. 5. In the temperature range between 300 K and 1000 K, the Seebeck coefficients of all the samples were positive and indicating a feature of n-type semiconductors. It can be seen from the figure that the doped of second element did not change the trend of the S - T curves. CDM has a relatively large absolute Seebeck coefficient, almost $-160 \mu\text{V K}^{-1}$ at 973 K. The introduction of second elements makes the Seebeck coefficient of the dual doped sample decrease. This phenomenon is attributed to the increase of carrier concentration. The Seebeck coefficient depends on concentration of charge carriers, which means that the all dual-doped samples may have similar carrier concentrations, and the similarity of the resistivity of the confirmation. The measurements of Hall coefficients also verify that the resistivity and Seebeck coefficient of the three samples have a similar trend, and the conclusion is reasonable, we can draw the conclusion that the second additional element introduces larger carrier concentration. Similar conclusions have been reported yet.^{11,19}

The Seebeck coefficient of CDM samples tends to saturation at 900 K, other three samples only observed at 750 K. From the theory of Heikes and Ure,²¹ the Fermi energy E_F has a narrow conducting band around it. Their research shows us that the

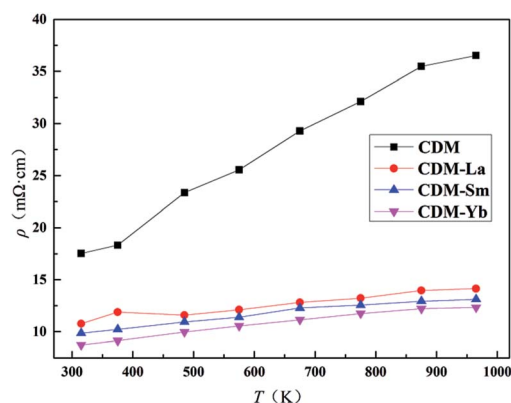
**Fig. 3** Temperature dependence of electrical resistivity for $\text{Ca}_{0.98}\text{Er}_{0.02}\text{MnO}_3$ and $\text{Ca}_{0.96}\text{Er}_{0.02}\text{Re}_{0.02}\text{MnO}_3$ (Re = La, Sm, Yb).

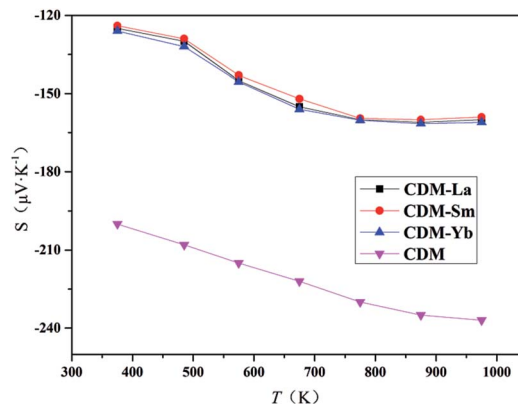
Table 3 Electrical conductivity (σ), Hall coefficient (R_H), carrier concentration (n), mobility (μ) at 300 K

Sample	σ (S cm ⁻¹)	$n \times 10^{18}$ (cm ⁻³)	R_H (cm ³ C ⁻¹)	μ (cm ² V ⁻¹ s ⁻¹)
CDM	56.9	91.23	0.068	3.89
CDM-La	92.7	130.53	0.047	4.43
CDM-Sm	101.4	141.65	0.044	4.48
CDM-Yb	114.1	147.82	0.042	4.81

Seebeck coefficient of a narrow band is predicted to saturate and become temperature-independent when the temperature is high enough that $k_B T$ is larger than the width of the band.²¹ The saturating temperature T_s is proportional to the width of the narrow band,²¹ which is about at 900 K for CDM and for dual doped samples are about at 750 K. Thus, when the second elements are doped, the conduction band becomes narrower. The similar reports could be found in other manuscripts by Wang *et al.*^{13–15}

It can be seen from Fig. 5 that the absolute value of the single-doped Seebeck coefficient is higher than that of the dual-doped in the entire test temperature range. At high temperatures, the material is restricted by Heikes. The Seebeck coefficient at the high-temperature limit is inversely proportional to the carrier concentration, the negative Seebeck values indicate that electron carriers dominate the whole system. With the introduction of the second element, the electron concentration in the material gradually increases, so that the Seebeck coefficient gradually decreases. $\text{Ca}_{0.96}\text{Er}_{0.02}\text{Re}_{0.02}\text{MnO}_3$ samples have the same Re^{3+} content, and the trend of the Seebeck coefficient is basically the same, so we can conclude that at high temperatures, the system's Seebeck is mainly dependent on the electron concentration.

The power factor is calculated through the conductivity and Seebeck coefficient. The temperature dependence of the power factor is shown in Fig. 6. The power factors increase with introduction of a second additional element into CDM. The highest values for CDM, CDM-La, CDM-Sm, and CDM-Yb were $217 \mu\text{W} (\text{K}^2 \text{m})^{-1}$, $193 \mu\text{W} (\text{K}^2 \text{m})^{-1}$, $202 \mu\text{W} (\text{K}^2 \text{m})^{-1}$,

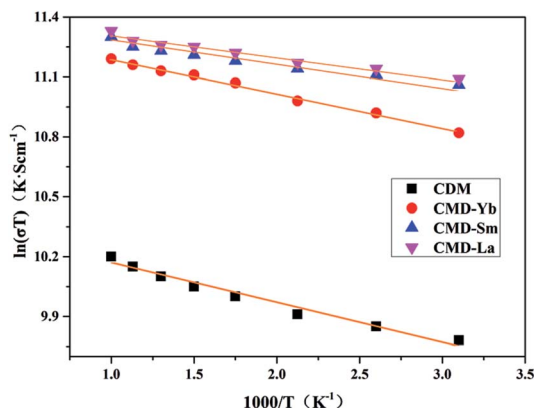
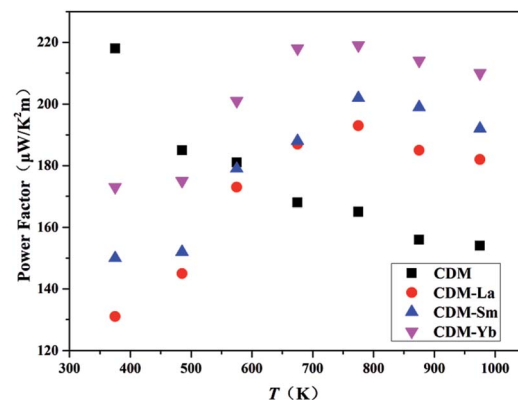
**Fig. 5** Temperature dependence of Seebeck coefficients for $\text{Ca}_{0.98}\text{Er}_{0.02}\text{MnO}_3$ and $\text{Ca}_{0.96}\text{Er}_{0.02}\text{Re}_{0.02}\text{MnO}_3$ (Re = La, Sm, Yb).

$219 \mu\text{W} (\text{K}^2 \text{m})^{-1}$, respectively, and CDM-Yb has the highest power factor in all samples.

Fig. 7 shows the thermal conductivity (κ) of all samples from 300 K to 1000 K. The minimum thermal conductivity of CDM is $2.45 \text{ W m}^{-1} \text{ K}^{-1}$ at 973 K. CDM-La, CDM-Sm, and CDM-Yb, the lowest values are obtained $1.81 \text{ W m}^{-1} \text{ K}^{-1}$, $1.72 \text{ W m}^{-1} \text{ K}^{-1}$, $1.68 \text{ W m}^{-1} \text{ K}^{-1}$, respectively, at 973 K. It can be seen from Fig. 7 that the thermal conductivity of the different dual-doped samples is very close and the values differ by 8% to 12%, but the sample of the dual-doped than single doped show smaller thermal conductivity. The results show that the dual-doped more effectively reduce the thermal conductivity for the CaMnO_3 system. As we all know that the total thermal conductivity (κ) can be expressed as the sum of the electronic thermal conductivity (κ_{ele}) and the phonon thermal conductivity (κ_{ph}). Where κ_{ph} is the contribution from phonons and κ_{ele} is the contribution from carriers. The electronic thermal conductivity is determined by the Wiedemann–Franz law:

$$\kappa_{\text{ele}} = LT/\rho \quad (2)$$

where $L = 2.45 \times 10^{-8} \text{ W } \Omega \text{ K}^{-2}$ is the Lorenz number, ρ is the electrical resistivity, and T is the absolute temperature. According to the Fig. 7, the thermal conductivity mainly comes

**Fig. 4** Relationship of $\ln(\sigma T)$ and $1000/T$.**Fig. 6** Temperature dependence of the power factor.

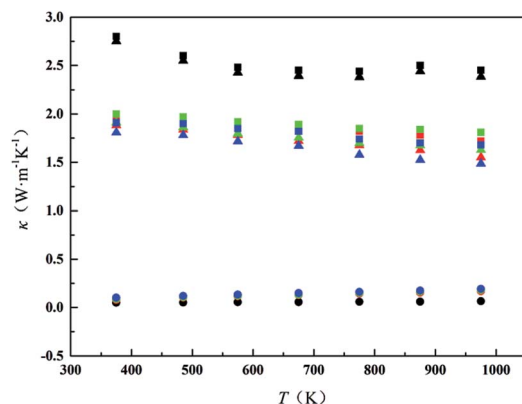


Fig. 7 Temperature dependence of total κ (■), electronic thermal conductivity κ_{ele} (●), and phonon thermal conductivity κ_{ph} (▲) for $\text{Ca}_{0.98}\text{Er}_{0.02}\text{MnO}_3$ (black symbols) and $\text{Ca}_{0.96}\text{Er}_{0.02}\text{Re}_{0.02}\text{MnO}_3$ (Re = Sm, La, Yb) (red, green, blue symbols), respectively.

from the phonon thermal conductivity, which can be supposed that the phonon thermal conductivity still contributes the most in the whole system. According to the report, the low thermal conductivity is mainly caused by distortion of lattice vibrations for doping samples. One is the weight of Re^{3+} higher than that of Ca^{2+} , the heavier weight leads to its vibration amplitude becomes smaller, the crystal of its lattice is relatively independent of the surrounding other lattice, the formation of strong localized vibration, resulting in lower phonon thermal conductivity. Secondly, the crystallographic distortion leads to the distortion of the lattice constant, which will hinder the propagation of phonons in the lattice and further reduce the phonon thermal conductivity.¹⁰ The reduction of phonon thermal conductivity directly leads to the decrease of total thermal conductivity.

Temperature dependence of dimensionless figure-of-merit ZT is shown in Fig. 8. The figure of merit ZT is an important parameter in evaluating the thermoelectric property of materials. As the test temperature increases, the values of ZT for all of the samples increase in the whole test temperature range. The ZT values of CDM-La, CDM-Sm, and CDM-Yb are almost higher

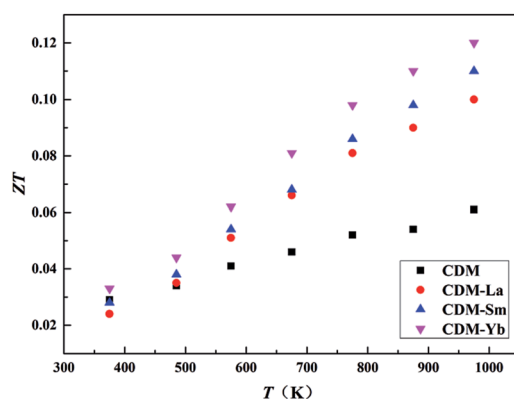


Fig. 8 Temperature dependence of the dimensionless figure-of-merit ZT .

than that of CDM. The highest figure of merit ZT exceeds 0.12 at 973 K for CDM-Yb, which represents 50% improvement compared with single dysprosium-doped sample CDM. And it shows that these manganites could be good candidates as n-type materials for high-temperature thermoelectric application.

4. Conclusions

A series of perovskite-type ceramic materials $\text{Ca}_{0.98}\text{Er}_{0.02}\text{MnO}_3$ and $\text{Ca}_{0.96}\text{Er}_{0.02}\text{Re}_{0.02}\text{MnO}_3$ (Re = La, Sm, Yb) which worked from 300 K to 1000 K with excellent thermoelectric properties was prepared sol-gel and cold-pressing method. Dual-doped is a very effective way to reduce the electrical resistivity and keeps a moderate absolute Seebeck coefficient. The introduction of second element leads to a remarked lower thermal conductivity. The highest figure of merit ZT exceeds 0.12 at 973 K for $\text{Ca}_{0.96}\text{Er}_{0.02}\text{Yb}_{0.02}\text{MnO}_3$ and it is about 50% improved compared with $\text{Ca}_{0.98}\text{Er}_{0.02}\text{MnO}_3$ sample at the same temperature. The results confirmed that dual-doping improved thermal electric properties of $\text{Ca}_{0.98}\text{Er}_{0.02}\text{MnO}_3$ efficiently.

Conflicts of interest

There are no conflicts to declare.

Acknowledgements

The work is financially supported by the Petroleum Production Engineering Institute Fund of Daqing Oil Field Limited Company, China (No. DQYT-1204003-2015-JS-824).

Notes and references

- 1 X. Zhang, X. Y. Ma, F. P. Zhang, P. X. Wu, Q. M. Lu, Y. Q. Liu and J. X. Zhang, *Acta Phys. Sin.*, 2012, **61**, 273–335.
- 2 Y. H. Lin, J. Lan, Z. Shen, Y. Liu, C. W. Nan and J. F. Li, *Appl. Phys. Lett.*, 2009, **94**, 425.
- 3 J. Han, Q. Sun and Y. Song, *J. Alloys Compd.*, 2017, **705**, 22–27.
- 4 Y. N. Huang, B. C. Zhao, S. Lin and Y. P. Sun, *J. Alloys Compd.*, 2017, **705**, 745–748.
- 5 H. C. Wang and C. L. Wang, *Mater. Res. Bull.*, 2012, **47**, 2252–2256.
- 6 F. P. Zhang, X. Zhang, Q. M. Lu, J. X. Zhang and Y. Q. Liu, *J. Alloys Compd.*, 2011, **509**, 4171–4175.
- 7 J. L. Lan, Y. H. Lin, H. Fang, A. Mei, C. W. Nan, Y. Liu, S. L. Xu and M. Peters, *J. Am. Ceram. Soc.*, 2010, **93**, 2121–2124.
- 8 H. Muguerra, B. Rivas-Murias, M. Traianidis, C. Marchal, P. Vanderbenden, B. Vertruyen, C. Henrist and R. Cloots, *J. Alloys Compd.*, 2011, **509**, 7710–7716.
- 9 T. Kobayashi, H. Takizawa, T. Endo, T. Sato, M. Shimada, H. Taguchi and M. Nagao, *J. Solid State Chem.*, 1991, **92**, 116–129.
- 10 M. Ohtaki, H. Koga, T. Tokunaga, K. Eguchi and H. Arai, *J. Solid State Chem.*, 1995, **120**, 105–111.



- 11 A. Kosuga, Y. Isse, Y. F. Wang, K. Koumoto and R. Funahashi, *J. Appl. Phys.*, 2009, **105**, 804.
- 12 D. Flahaut, T. Mihara, R. Funahashi, N. Nabeshima, K. Lee, H. Ohta and K. Koumoto, *J. Appl. Phys.*, 2006, **100**, 2331.
- 13 Y. Wang, Y. Sui and W. H. Su, *J. Appl. Phys.*, 2008, **104**, 93703.
- 14 Y. Wang, Y. Sui, H. J. Fan, X. J. Wang, Y. T. Su, W. H. Su and X. Y. Liu, *Chem. Mater.*, 2009, **21**, 4653–4660.
- 15 Y. Wang, Y. Sui, X. J. Wang and W. H. Su, *Appl. Phys. Lett.*, 2010, **97**, 1457.
- 16 C. J. Liu, A. Bhaskar and J. J. Yuan, *Appl. Phys. Lett.*, 2011, **98**, 214101.
- 17 A. Bhaskar, C. J. Liu and J. J. Yuan, *J. Electron. Mater.*, 2012, **41**, 2338–2344.
- 18 Y. H. Zhu, C. L. Wang, W. B. Su, J. C. Li, J. Liu, Y. L. Du and L. M. Mei, *Ceram. Int.*, 2014, **40**, 15531–15536.
- 19 Y. H. Zhu, C. L. Wang, H. C. Wang, W. B. Su, J. Liu and J. C. Li, *Mater. Chem. Phys.*, 2014, **144**, 385–389.
- 20 R. D. Shannon, *Acta Crystallogr.*, 1976, **32**, 751–767.
- 21 R. P. Heikes and R. W. Ure, *Thermoelectricity*, Interscience, New York, 1961.
- 22 Y. H. Zhu, W. B. Su, J. Liu, Y. C. Zhou, J. C. Li, X. H. Zhang, Y. L. Du and C. L. Wang, *Ceram. Int.*, 2015, **41**, 1535–1539.
- 23 R. Kabir, R. M. Tian, T. S. Zhang, R. Donelson, T. T. Tan and S. Li, *J. Alloys Compd.*, 2015, **628**, 347–351.
- 24 A. Hmood, A. Kadhim and H. Abu Hassan, *Mater. Chem. Phys.*, 2012, **136**, 1148–1155.
- 25 A. Kadhim, A. Hmood and H. Abu Hassan, *Mater. Sci. Semicond. Process.*, 2013, **16**, 537–541.

